Environmental Science: Atmospheres

ROYAL SOCIETY OF CHEMISTRY

PAPER

View Article Online
View Journal | View Issue

Cite this: *Environ. Sci.: Atmos.*, 2024, **4**, 813

Towards a better understanding of the HO_2 uptake coefficient to aerosol particles measured during laboratory experiments

P. S. J. Lakey [ab] T. Berkemeier [c] M. T. Baeza-Romero [d] U. Pöschl [c] M. Shiraiwa [b] and D. E. Heard [*a]

The first measurements of HO_2 uptake coefficients (γ_{HO_2}) onto suspended aerosol particles as a function of temperature are reported in the range 314 K to 263 K. For deliquesced ammonium nitrate (AN) particles γ_{HO_2} increases from 0.005 ± 0.002 to 0.016 ± 0.005 as the temperature is lowered over this range. For effloresced sodium chloride and ammonium sulphate particles, γ_{HO_2} decreases slightly from 0.004 ± 0.002 to 0.000 ± 0.002 and 0.002 ± 0.003, respectively, between 314 and 263 K. For AN particles doped with Cu^{2+} ions, we find $\gamma_{HO_2} \approx \alpha_{HO_2}$, the mass accommodation coefficient, which increases very slightly from $\alpha_{HO_2} = 0.62 \pm 0.05$ to 0.71 ± 0.06 between 292 and 263 K with lowering temperature. New measurements of γ_{HO_2} are also reported for ammonium sulphate particles doped with a range of Fe^{2+} and Fe^{3+} concentrations. The dependence of γ_{HO_2} on Cu and Fe concentrations are reconciled with published rate coefficients using the kinetic multi-layer model of aerosol surface and bulk chemistry (KM-SUB). The model shows that in experimental studies using aerosol flow tubes, a time dependence is expected for γ_{HO_2} onto aerosol particles which do not contain transition metal ions due to a decrease in the gas-phase concentration of HO_2 as a function of time. The model also demonstrates that Fenton-like chemistry has the potential to decrease γ_{HO_2} as a function of time for particles containing transition metal ions. For atmospherically relevant transition metal ion concentrations in aerosol particles, γ_{HO_2} can take a range of values depending on pH and the particle size from $\gamma_{HO_2} < 0.04$ to $\gamma_{HO_2} = \alpha_{HO_2}$. γ_{HO_2} for larger particles (radius ≥ 0.5 μm) can be significantly reduced by gas-diffusion limitations.

Received 1st March 2024
Accepted 8th June 2024

DOI: 10.1039/d4ea00025k

rsc.li/esatmospheres

Environmental significance

HO_2 plays a crucial role in the oxidation chemistry of the atmosphere, but the numerical value of its uptake coefficient (γ_{HO_2}) that is used in atmospheric modelling remains uncertain. In this study, experiments indicate that γ_{HO_2} for deliquesced and effloresced particles will increase with decreasing temperature. Literature rate coefficients are included in a kinetic model to better understand measured γ_{HO_2} trends as a function of time, gas-phase concentrations of HO_2, and particle-phase concentrations of transition metal ions. The model demonstrates that γ_{HO_2} can vary significantly for different atmospherically relevant particles, reveals important factors that control γ_{HO_2}, and identifies further experiments that could be performed to resolve uncertainties.

1. Introduction

OH and HO_2 radicals (collectively known as HO_x) control the oxidative capacity of the troposphere and hence the lifetimes and concentrations of many trace species within the troposphere, such as NO_x (NO and NO_2) and volatile organic compounds (VOCs). The reaction of HO_2 with NO is a major source of ozone, which can damage vegetation, is a respiratory irritant and a greenhouse gas.[1,2] Gas-phase reactions controlling HO_x concentrations have been extensively studied, and recommendations for rate coefficients, product branching ratios and photochemical parameters such as absorption cross-sections and photolysis quantum yields have been made for the wider community in models by panels of experts.[3–5] Although there is also an IUPAC recommendation for heterogeneous reactions which includes HO_2 uptake to aerosol particles,[6] there remain uncertainties in processes which control the uptake coefficient γ_{HO_2}. Over more than two decades, measurements during field campaigns, particularly at lower levels of NO_x, have often shown lower HO_2 concentrations than predicted by box models containing a mechanism for gas-phase reactions and which have been constrained to other measured species.[7–23] The

[a]*School of Chemistry, University of Leeds, Woodhouse Lane, Leeds, LS2 9JT, UK. E-mail: d.e.heard@leeds.ac.uk*

[b]*Department of Chemistry, University of California, Irvine, CA 92697, USA*

[c]*Max-Planck Institute for Chemistry, Multiphase Chemistry Department, Hahn-Meitner-Weg 1, 55128 Mainz, Germany*

[d]*Department of Physical Chemistry, School of Industrial and Aerospace Engineering, Institute of Nanoscience, Nanotechnology and Molecular Materials, Universidad de Castilla-La Mancha, 45071, Toledo, Spain*

overprediction by the models has often been attributed, at least in part, to HO_2 uptake by aerosol particles, although for some earlier studies in coastal regions this conclusion was reached when HO_2 loss *via* reactions with halogen oxides was not recognised and hence not included in the model.

Parameterisations of γ_{HO_2} for use in atmospheric models have been suggested for a number of modelling studies.[24,25] Modelling studies often use a single value of $\gamma_{HO_2} = 0.2$ (*e.g.* Jacob[26]), and studies using the GEOS-Chem model suggested that increases in ozone levels in China were driven by the decrease in levels of $PM_{2.5}$ in response to government legislation, because $PM_{2.5}$ scavenges HO_2 which would otherwise react with NO_x to generate O_3.[25] Song *et al.*[27] recently developed a new parameterisation for γ_{HO_2} that depends both on measured concentrations of Cu^{2+} within field-sampled aerosol particles and the aerosol liquid water content, the latter calculated from the measured relative humidity (RH). The parameterisation was applied in a multiphase reaction kinetic model, which predicts values of γ_{HO_2} that varied significantly during a given field campaign, suggesting a single value of γ_{HO_2} is not appropriate.[27,28] Moreover, several field measurements of HO_2 in China together with modelling studies, some of which utilise this new parameterisation, do not support an important role for heterogeneous uptake of HO_2 except under low concentrations of NO_x.[27,29] Guo *et al.*[30] reported a theoretical evaluation of the roles of several factors which control γ_{HO_2} for spherical aerosol particles containing a range of Cu^{2+} ion concentrations. The study also showed that the use of a single value of γ_{HO_2} for aerosol particles of different size, composition or physical state was not appropriate, and concluded that both careful selection of the appropriate value of γ_{HO_2} should be made for modelling studies and that further laboratory measurements are needed. However, this theoretical analysis is based on a modified resistor model with some limitations; for example, it does not take into account second-order reactions of HO_2 nor the presence of any pH gradient inside of the aerosol particle due to reaction. Similarly, Li *et al.*[31] also recently used a resistor model to investigate the effect of variables such as the HO_2, Fe and Cu concentrations on γ_{HO_2} and demonstrated that a wide range of γ_{HO_2} values were expected.

Taketani *et al.*[32] measured values of γ_{HO_2} from 0.09–0.40 from regenerated aerosol particles of water extracts from ambient aerosol particles at two mountain sites in China, which together with aerosol composition measurements suggested a key role for transition metals in controlling HO_2 uptake. Recently Zhou *et al.* reported values of γ_{HO_2} using online HO_2 reactivity measurements under ambient conditions in two Japanese cities with a system that enriches ambient aerosol particles.[33–35] Using an auto-switching aerosol filter, Zhou *et al.* were able to isolate the loss of HO_2 due to heterogeneous uptake, with an average γ_{HO_2} of 0.24, but displaying considerable variability, and concluding that a single value of γ_{HO_2} should not be used in modelling studies. Using a chemical transport model, Ivatt *et al.*[36] showed that for some parts of the world the dominant chain termination reaction was not reaction of OH with NO_2 to form nitric acid, nor reaction of RO_2 with HO_2 to form peroxides, but rather the reactive removal of HO_2 onto aerosol surfaces, placing these regions into a new "aerosol inhibited" photochemical regime.

There are still relatively few laboratory studies that have investigated the γ_{HO_2} for different types of aerosol particles, with a large variance in the values reported. Small uptake coefficients are reported in some studies for effloresced (solid, $\gamma_{HO_2} < 0.004$) and deliquesced (aqueous, $0.004 < \gamma_{HO_2} < 0.02$) aerosol particles containing organic compounds and inorganic salts.[37–39] However, other studies have measured much larger γ_{HO_2} for these solid ($\gamma_{HO_2} < 0.01$–0.05) and aqueous ($\gamma_{HO_2} = 0.09$–0.19) aerosol particles.[39–42] Li *et al.*[31] have recently demonstrated that differences in γ_{HO_2} between studies may be in part due to different experimental HO_2 concentrations. Lakey *et al.*[43] reported a large difference (~4 orders of magnitude) between rate coefficients of aqueous phase HO_2/O_2^- and Cu^+/Cu^{2+} published in the literature,[43,44] and those required to fit γ_{HO_2} measurements for aerosol particles containing a range of copper ion concentrations. Additional measurements of γ_{HO_2} as a function of Cu and Fe concentrations have recently been published, demonstrating that Cu must be greater than 10^{-5} M to significantly increase γ_{HO_2}.[27,31,42] By assuming a low pH ~ 4 and a smaller rate coefficient (1.5×10^7 M^{-1} s^{-1}) between Cu^{2+} ions and HO_2/O_2^- than had previously been used (8×10^9 M^{-1} s^{-1}), studies have been able to reproduce the increasing uptake coefficients with an increase of Cu concentrations.[27,31] Li *et al.*[31] were also able to reproduce an Fe-doped experiment by similarly lowering the rate coefficient between Fe^{3+} and HO_2/O_2^-. It has been suggested that the lower rate coefficient between Cu^{2+} and HO_2/O_2^- may reflect the overall rate coefficient expected in more acidic environments.[27,31,45]

A time dependence and a HO_2 concentration dependence of γ_{HO_2} during some experiments[38,46] have been observed, raising the question of which value should be used within an atmospheric model. A larger value of γ_{HO_2} was measured at lower HO_2 concentrations, which is inconsistent with the assumption that the uptake is controlled by HO_2 self-reaction within the aerosol particle.[38,47] Thus, there are still uncertainties regarding γ_{HO_2} in terms of discrepancies between field measurements and model calculations, different laboratory studies and reported rate coefficients of HO_2/O_2^- with Cu^+/Cu^{2+} in the aqueous phase.

Previous studies[48–50] measured the uptake coefficient of HO_2 at low total pressure (1–3 torr in He) on dry surfaces or solid films of ammonium nitrate, sodium chloride and bromide, and magnesium chloride over a range of temperatures between 240–345 K, with the uptake coefficient decreasing significantly with increasing temperature. There have also been several studies of γ_{HO_2} onto sulphuric acid aerosol particles at room temperature[39] as well as onto surfaces coated with sulphuric acid at lower temperatures.[51–53] The γ_{HO_2} onto sulphuric acid also appeared to be temperature dependent with an uptake coefficient of <0.01 and >0.2 measured at 295 K and 243 K, respectively. Field measurements have shown that a larger γ_{HO_2} is required to explain the difference between measured and predicted HO_2 concentrations at low temperatures.[15,47] However, to the best of our knowledge, currently there is no study

investigating the temperature dependence of γ_{HO_2} onto suspended deliquesced and effloresced aerosol particles.

In this paper we report the first systematic measurements of γ_{HO_2} for effloresced and deliquesced ammonium nitrate, sodium chloride and ammonium sulphate aerosol particles as a function of temperature. Measurements of γ_{HO_2} for $(NH_4)_2SO_4$ particles containing variable concentrations of $CuSO_4$, $FeSO_4$ and $(NH_4)_2Fe(SO_4)_2$ are also made. In addition, a simplified mechanism for aerosol uptake of HO_2 incorporated within the kinetic multi-layer model of aerosol surface and bulk chemistry (KM-SUB) is used to examine the chemical and physical processes that control γ_{HO_2}, to rationalize uncertainties and compare the measurements in this work with earlier studies.[27,31,38–40,42,43]

2. Methods

2.1. General description of apparatus

Experiments were performed using the setup first described by George *et al.*[38] and used in other studies,[37,43,46,54] and only a brief description is given here. Atomizer solutions used to generate aerosol particles were prepared by dissolving 5 grams of either sodium chloride (Fisher, 99.9%) or ammonium nitrate (Fisher, 99.9%) into 500 ml Milli-Q water. For some experiments, copper sulphate, iron sulphate or ammonium iron sulphate (Fisher 99.8%) was also added to the atomizer solutions. The concentration of copper and iron in the aerosol particles were estimated from the atomizer concentration solutions following the methodology described in Section 2.2. Aerosol particles were generated from these solutions in a flow of N_2 using an atomizer (TSI 3076), and passed through a neutralizer (Grimm 5522), an impactor (TSI 1035900, 0.071 cm pinhole) and a HEPA (High Efficiency Particulate Air) filter/bypass allowing the particle concentration to be altered. Subsequently, the particle flow (1.0 $\pm$ 0.1 slpm) was mixed with a humidified flow of N_2 (3.0 $\pm$ 0.1 slpm) in a conditioning flow tube for ~10 seconds before entering the reaction flow tube. The size-resolved aerosol particle concentration was measured using a Scanning Mobility Particle Sizer (SMPS, TSI 3080) after the flow tube.

HO_2 radicals were formed by the photolysis of water vapour over a mercury lamp (L.O.T. Oriel, model 6035) in the presence of trace amounts of oxygen as shown below:

$$H_2O + h\nu\ (193\ nm) \rightarrow OH + H \quad (R1)$$

$$H + O_2 + M \rightarrow HO_2 + M \quad (R2)$$

The mercury lamp was placed at the end of the injector furthest away from the reaction flow tube to reduce localized heating within the flow tube. The injector flow (1.32 $\pm$ 0.05 slpm), which contained the HO_2 radicals, was released perpendicularly *via* several small holes into the main flow within the reaction flow tube. At the end of the flow tube, the HO_2 radicals were sampled by a 1 mm diameter pinhole and entered a Fluorescence Assay by Gas Expansion (FAGE) detector, where they reacted with an excess of added NO to form OH radicals that were then detected by laser induced fluorescence (LIF) spectroscopy using the $Q_1(2)$ transition of the $A^2\Sigma^+(v' = 0) \leftarrow X^2\Pi_i\ (v'' = 0)$ band at ~308 nm.[20,55] The FAGE detector was kept at low pressure (~0.85 torr) using a combination of a rotary pump (Edwards, model E1M80) and a roots blower (EH1200). The relative HO_2 LIF signal was converted to an absolute concentration following a calibration with a known concentration of HO_2. The initial HO_2 concentration exiting the moveable injector was varied by altering the current supplied to the mercury lamp and after dilution with the main flow was in the range ~2.4×10^8 cm^{-3} to ~2.7×10^9 cm^{-3}.

Two experimental methodologies were used to measure the HO_2 uptake coefficient, γ_{HO_2},[38] referred to as the 'moving injector' method and the 'fixed injector' method. For 'moving injector' experiments, the injector that released the HO_2 radicals was moved backwards and forwards along the reaction flow tube and the decay of HO_2 measured both in the absence of and presence of different aerosol particle number concentrations. The decays were performed for reaction times between 10 to 20 seconds, with time zero defined as when HO_2 is injected into the main flow, allowing time for full mixing. For 'fixed injector' experiments the injector was placed in 6 different positions along the flow tube (equivalent to reaction times of ~5, 8, 11, 14, 17 and 20 seconds) and the HO_2 signal was measured as the aerosol particle concentration in the flow tube was changed. The main difference between these two methodologies is that for the 'moving injector' experiments the measured γ_{HO_2} is equivalent to the average γ_{HO_2} for a reaction time between 10–20 seconds, whereas for the 'fixed injector' experiments γ_{HO_2} is equivalent to the average γ_{HO_2} between 0 seconds (point of mixing of HO_2 and aerosol particles) and the reaction time corresponding to the fixed position of the injector.

2.2. Moving injector experiments

For 'moving injector' experiments (which is the methodology used for the majority of HO_2 aerosol uptake experiments), the HO_2 decay along the flow tube in the absence and presence of different aerosol particle concentrations was assumed to follow first-order kinetics as follows:

$$\ln[HO_2]_t = \ln[HO_2]_0 - k_{obs}t \quad (E1)$$

where $[HO_2]_t$ is the HO_2 concentration at time t, $[HO_2]_0$ is the initial HO_2 concentration and k_{obs} is the observed pseudo-first order rate coefficient. In the absence of aerosol particles $k_{obs} = k_{wall}$. The $k_{obs} - k_{wall}$ rate coefficients were corrected to k' in order to take into account non-plug flow conditions within the flow tube using the method described by Brown.[56] The Brown correction meant that on average k' was 35% larger than $k_{obs} - k_{wall}$. The k' values were related to γ_{HO_2} by:

$$k' = \frac{\gamma_{HO_2}\omega_{HO_2}}{4}S \quad (E2)$$

where w_{HO_2} is the molecular velocity of HO_2 and S is the total aerosol particle surface area. Finally, γ_{HO_2} was corrected for gas-phase diffusion limitations using the methodology described by Fuchs and Sutugin[57] and this correction changed γ_{HO_2} by less than 1%.

2.3. Fixed injector experiments

For 'fixed injector' experiments the injector was placed in one position at a time and the HO_2 signal was recorded whilst the aerosol particle concentration was varied. The HO_2 signal when aerosol particles were present could be described by the following equation:

$$\frac{\ln[HO_2]_{t,\text{aerosol}} - \ln[HO_2]_0}{t} = -k_{\text{aerosol}} - k_{\text{wall}} \quad \text{(E3)}$$

where $[HO_2]_0$ and $[HO_2]_{t,\text{aerosol}}$ are the HO_2 concentration at time zero and at time t for a given aerosol particle concentration, respectively. Similarly, the signal without any aerosol particles present can be described as:

$$\frac{\ln[HO_2]_{t,\text{aerosol}=0} - \ln[HO_2]_0}{t} = -k_{\text{wall}} \quad \text{(E4)}$$

Subtraction of (E3) and (E4) gives:

$$\frac{\ln[HO_2]_{t,\text{aerosol}} - \ln[HO_2]_{t,\text{aerosol}=0}}{t} = -k_{\text{aerosol}} \quad \text{(E5)}$$

Therefore, for a given injector position, dividing $\ln[HO_2]_{t,\text{aerosol}=0} - \ln[HO_2]_{t,\text{aerosol}}$ by t gives a value of k_{aerosol} for each aerosol particle surface area concentration. The Brown correction was then applied to obtain k' and eqn (E2) was used to obtain γ_{HO_2}, which was then corrected for gas phase diffusion limitations, but as for the moving injector experiments this changed the values by less than 1%.

A range of moving and fixed injector experiments were performed for a range of experimental conditions.

2.4. Temperature-dependent experiments of γ_{HO_2}

For some experiments the temperature was varied between −10 °C (263 K) and 40 °C (313 K) by flowing a 50 : 50 mixture of water and ethylene glycol, which had been cooled or heated using a refrigerated circulator (Thermo Scientific Haake, DC50-K35), through the jackets of both the conditioning flow tube and the main flow tube. Any axial or radial temperature gradients were measured within the flow tube, both along the top edge next to the jacket and along the centre of the flow tube using moveable thermocouples. As shown in Fig. 1, the temperature gradients are small, within 1 °C for almost the whole flow tube.

Initially, attempts were made to place the entire Differential Mobility Analyser (DMA) in a freezer to maintain its temperature and relative humidity to be same as in the aerosol flow tube. However, temperature gradients developed in the freezer leading to convection within the DMA and no aerosol particles were measured. Therefore, the DMA was always kept at room temperature whilst the temperature in the conditioning and reaction flow tubes was varied. When the flow tube was not at room temperature, the relative humidity within it was different to the relative humidity in the DMA that was always kept at room temperature. When the flow tube was at a temperature that was lower than room temperature, the relative humidity in the flow tube would be greater than in the DMA, and therefore

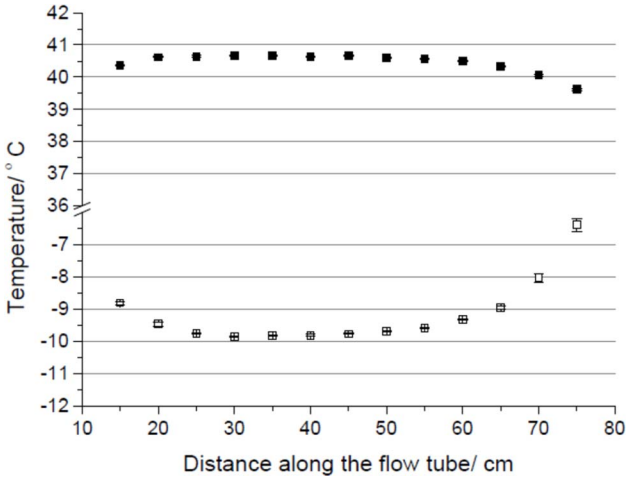

Fig. 1 Temperature gradients along the flow tube when the chiller was set to −10 °C and 40 °C (the two extreme temperatures). The injector tip was radially centered and placed at 75 cm from the end of the flow tube, which was open to the atmosphere at 0 cm. The flows were the same as the flows used during experiments.

the total aerosol particle surface area would be larger in the flow tube than the surface area measured by the SMPS. Alternatively, when the flow tube was at a temperature that was higher than room temperature, the humidity in the flow tube was lower than in the DMA, which meant that the total aerosol particle surface area in the flow tube was smaller than the surface area measured by the SMPS. Therefore, when experiments were performed with aqueous aerosol particles at temperatures different to room temperature, a correction in the total aerosol particle surface area had to be made.

The Extended Aerosol Inorganic Model (E-AIM)[58–60] can calculate the molar volume of an aqueous salt solution as a function of temperature and humidity at thermodynamic equilibrium. This model was run for the conditions in both the aerosol flow tube and the DMA. The following methodology was then used to correct the measured surface area in the SMPS to what it would have been within the aerosol flow tube.

Aqueous aerosol particles were assumed to be spherical and by using E-AIM to obtain the molar volume of an aqueous salt solution at different humidities the fractional change in volume is given by:

$$\frac{V_1}{V_2} = \frac{{r_1}^3}{{r_2}^3} \quad \text{(E6)}$$

where V_1 is the volume for one mole of salt per cubic centimetre at the flow tube temperature and humidity, V_2 is the volume for one mole of salt per cubic centimetre at the DMA temperature and humidity. The fractional change in surface area can similarly be given by:

$$\frac{S_1}{S_2} = \frac{r_1^2}{r_2^2} \quad \text{(E7)}$$

where S_1 is the aerosol particle surface area in the flow tube and S_2 is the aerosol particle surface area measured in the DMA.

Therefore, by combining eqn (E6) and (E7), gives:

$$S_1 = S_2\sqrt[3]{\left(\frac{V_1}{V_2}\right)^2} \quad \text{(E8)}$$

Eqn (E8) enables a correction for the total surface area of the aerosol particles when measured at a different humidity to that in the flow tube. For example, for a specific experiment performed using NaCl aerosol particles with the flow tube at 0 °C and the DMA at 20 °C, the relative humidity in the DMA was 18% compared to a relative humidity of 48% in the flow tube. This led to a 15% increase in the aerosol particle surface area measured by the SMPS. The flow rate and volume of the gas within the flow tube was also corrected to take into account the temperature.

It should be noted that the correction to the aerosol particle surface area limited the range of aqueous (deliquesced) aerosol particles that could be investigated to ammonium nitrate, as it does not effloresce over the range of temperatures and relative humidities studied. Deliquesced copper-doped ammonium nitrate aerosol particles appeared to grow or shrink in a similar way to pure ammonium nitrate aerosol particles for a given temperature, so it is assumed that the same growth curve can be applied for doped and non-doped AN. However, this methodology could not be used to apply a correction between effloresced and deliquesced aerosol particles for sodium chloride and ammonium nitrate aerosol particles. Even at 10 °C, to keep the RH in the DMA over the efflorescence humidity of sodium chloride and ammonium nitrate, the RH in the flow tube reactor would have to exceed 100% RH. If the relative humidity in the flow tube exceeded 100% RH there would be condensation on the flow tube walls leading to high wall losses and the aerosol particles would grow to form droplets which would be likely to be deposited and would be too large to be measured by the SMPS. Note that a high relative humidity in the flow tube at an elevated temperature could potentially lead to condensation in the DMA and therefore inaccurate measurements. Below the deliquescence point the aerosol particle surface area does not change with relative humidity for effloresced salts, the surface area remains constant as there is no aqueous phase which can increase or decrease in volume as the humidity changes, and so no surface area correction was required. However, when effloresced salt experiments were performed at different temperatures (ammonium sulphate and sodium chloride), it had to be ensured that the effloresced aerosol particles were never exposed to humidities above their deliquescence point.

The temperature range that was investigated in this work (263–314 K) is relevant for the atmosphere. Measurements have not been made at lower temperatures due to lack of HO_2 sensitivity (due to higher wall losses), larger temperature gradients along the flow tube and droplet formation (since the RH exceeds 100%).

2.5. Description of the KM-SUB model

The kinetic multi-layer model of aerosol surface and bulk chemistry (KM-SUB) has previously been described in detail by Shiraiwa *et al.*[61] and the adaptations for HO_2 have also previously been outlined.[54] Therefore, the model is only briefly described below. The KM-SUB model for HO_2 uptake consists of different layers: a gas phase, a near-surface gas phase, a sorption layer and 100 bulk layers. Processes included within the model are gas-phase diffusion, adsorption and desorption to and from the surface of the aerosol particle, surface-bulk exchange, diffusion between the bulk layers of the aerosol particle as well as chemical reaction in the gas phase, the particle bulk, and on the walls of the flow tube. Each of these processes have been described in detail elsewhere.[61,62] We assumed that the aqueous chemistry shown by reactions (R3)–(R17) below occurred within the aerosol particles. In the model, a gas-phase loss of HO_2 *via* its self-reaction (reaction (R18)) and an uptake of HO_2 and H_2O_2 to the walls of the flow tube (Table 1) were included. For simplicity the pH in the aerosol particles was assumed to be constant without being influenced by the following reactions.

$$HO_{2(aq)} \rightleftharpoons H^+_{(aq)} + O_2^-{}_{(aq)} \quad K_{eq} \quad \text{(R3)}$$

$$HO_{2(aq)} + HO_{2(aq)} \rightarrow H_2O_{2(aq)} + O_{2(aq)} \quad k_{BR,4} \quad \text{(R4)}$$

$$HO_{2(aq)} + O_2^-{}_{(aq)} + H_2O_{(l)} \rightarrow H_2O_{2(aq)} + O_{2(aq)} + OH^-_{(aq)} \quad k_{BR,5} \quad \text{(R5)}$$

$$CuSO_{4(aq)} + HO_{2(aq)} \rightarrow O_{2(aq)} + Cu^+_{(aq)} + HSO_4^-{}_{(aq)} \quad k_{BR,6} \quad \text{(R6)}$$

$$CuSO_{4(aq)} + O_2^-{}_{(aq)} \rightarrow O_{2(aq)} + Cu^+_{(aq)} + SO_4^{2-}{}_{(aq)} \quad k_{BR,7} \quad \text{(R7)}$$

$$Cu^{2+}_{(aq)} + HO_{2(aq)} \rightarrow O_{2(aq)} + Cu^+_{(aq)} + H^+_{(aq)} \quad k_{BR,8} \quad \text{(R8)}$$

$$Cu^{2+}_{(aq)} + O_2^-{}_{(aq)} \rightarrow O_{2(aq)} + Cu^+_{(aq)} \quad k_{BR,9} \quad \text{(R9)}$$

$$Cu^+_{(aq)} + HO_{2(aq)} + H_2O_{(l)} \rightarrow H_2O_{2(aq)} + Cu^{2+}_{(aq)} + OH^-_{(aq)} \quad k_{BR,10} \quad \text{(R10)}$$

$$Cu^+_{(aq)} + O_2^-{}_{(aq)} + 2H_2O_{(l)} \rightarrow H_2O_{2(aq)} + Cu^{2+}_{(aq)} + 2OH^-_{(aq)} \quad k_{BR,11} \quad \text{(R11)}$$

$$H_2O_{2(aq)} + Cu^+_{(aq)} \rightarrow OH_{(aq)} + OH^-_{(aq)} + Cu^{2+}_{(aq)} \quad k_{BR,12} \quad \text{(R12)}$$

$$H_2O_{2(aq)} + CuSO_{4(aq)} \rightarrow HO_{2(aq)} + HSO_4^-{}_{(aq)} + Cu^+_{(aq)} \quad k_{BR,13} \quad \text{(R13)}$$

$$Fe(SO_4)^+_{(aq)} + HO_{2\,(aq)} \rightarrow O_{2\,(aq)} + Fe^{2+}_{(aq)} + SO_4^{2-}{}_{(aq)} + H^+_{(aq)} \quad k_{BR,14} \quad \text{(R14)}$$

$$Fe(SO_4)^+_{(aq)} + O_2^-{}_{(aq)} \rightarrow O_{2(aq)} + Fe^{2+}_{(aq)} + SO_4^{2-}{}_{(aq)} \quad k_{BR,15} \quad \text{(R15)}$$

$$Fe^{2+}_{(aq)} + HO_{2(aq)} + H_2O_{(l)} \rightarrow H_2O_{2(aq)} + Fe^{3+}_{(aq)} + OH^-_{(aq)} \quad k_{BR,16} \quad \text{(R16)}$$

$$Fe^{2+}_{(aq)} + O_2^-{}_{(aq)} + 2H_2O_{(l)} \rightarrow H_2O_{2(aq)} + Fe^{3+}_{(aq)} + 2OH^-_{(aq)} \quad k_{BR,17} \quad \text{(R17)}$$

$$HO_{2(g)} + HO_{2(g)} \rightarrow H_2O_{2(g)} + O_{2(g)} \quad k_{GP} \quad \text{(R18)}$$

Table 1 The parameters used within the KM-SUB model when fitting all experimental data at 293 K

Parameter	Description	Value	Reference or comment
K_{eq}	Equilibrium constant for reaction (R3)	2.1×10^{-5}	Thornton *et al.*[47]
$k_{BR,4}$	Rate coefficient for reaction (R4)	1.3×10^{-15} cm^3 s^{-1}	Thornton *et al.*[47]
$k_{BR,5}$	Rate coefficient for reaction (R5)	1.5×10^{-13} cm^3 s^{-1}	Thornton *et al.*[47]
$k_{BR,6}$[a]	Rate coefficient for reaction (R6)	1.7×10^{-14} cm^3 s^{-1}	Mao *et al.*[63]
$k_{BR,7}$[a]	Rate coefficient for reaction (R7)	1.7×10^{-13} cm^3 s^{-1}	Mao *et al.*[63]
$k_{BR,8}$[b]	Rate coefficient for reaction (R8)	1.7×10^{-13} cm^3 s^{-1}	Jacob[26]
$k_{BR,9}$[b]	Rate coefficient for reaction (R9)	1.3×10^{-11} cm^3 s^{-1}	Jacob[26]
$k_{BR,10}$	Rate coefficient for reaction (R10)	2.5×10^{-12} cm^3 s^{-1}	Jacob[26]
$k_{BR,11}$	Rate coefficient for reaction (R11)	1.6×10^{-11} cm^3 s^{-1}	Jacob[26]
$k_{BR,12}$	Rate coefficient for reaction (R12)	1.2×10^{-17} cm^3 s^{-1}	Deguillaume *et al.*[64] only included in Fig. 4(d)
$k_{BR,13}$	Rate coefficient for reaction (R13)	7.6×10^{-19} cm^3 s^{-1}	Pham *et al.*[65] only included in Fig. 4(d) same rate coefficient as for Cu^{2+} is assumed
$k_{BR,14}$	Rate coefficient for reaction (R14)	1.7×10^{-18} cm^3 s^{-1}	Rush and Bielski[66]
$k_{BR,15}$	Rate coefficient for reaction (R15)	2.5×10^{-13} cm^3 s^{-1}	Rush and Bielski[66]
$k_{BR,16}$	Rate coefficient for reaction (R16)	2.0×10^{-15} cm^3 s^{-1}	Jacob[26]
$k_{BR,17}$	Rate coefficient for reaction (R17)	1.7×10^{-14} cm^3 s^{-1}	Jacob[26]
γ_{wall}	Uptake coefficient of HO_2 and H_2O_2 onto the walls of the flow tube	6.50×10^{-6}	HO_2 uptake is consistent with the data. An assumption of no products is made
k_{GP}	Rate coefficient for HO_2 self-reaction in the gas phase	3×10^{-12} cm^3 s^{-1}	Sander *et al.*[67]
H_{HO_2}	Henry's law coefficient for HO_2	5600 M atm^{-1}	Thornton *et al.*[47]
$H_{H_2O_2}$	Henry's law coefficient for H_2O_2	1.65×10^5 M atm^{-1}	Staffelbach and Kok[68]
$D_{b,all}$	Diffusion coefficient for all species within the aerosol particle bulk	1×10^{-5} cm^2 s^{-1}	Thornton *et al.*[47]
$\alpha_{s,0}$	Surface accommodation coefficient[c] of HO_2 and H_2O_2	0.5	These values are used unless otherwise stated
r_p	Particle radius	50 nm	
$[HO_2]$	Initial HO_2 concentration	1×10^9 cm^{-3}	
τ_d	Desorption lifetime	1.0×10^{-11} s	
D_g	Gas phase diffusion coefficient of HO_2 and H_2O_2 in the gas phase	0.25 cm^2 s^{-1}	Thornton *et al.*[47]

[a] Note that the rate coefficients for $CuSO_4$ with O_2^-/HO_2 have not been directly measured and uncertainty remains with regards to their values. [b] The rate coefficients with free Cu^{2+} are only used in Fig. 4(c) and for comparison with $CuSO_4$ in Fig. 5(a). [c] The experimentally measured mass accommodation coefficients may be different from the surface accommodation coefficients if there are significant gas-phase diffusion limitations or if HO_2 diffusing into the bulk becomes a limiting process but should otherwise equal the surface mass accommodation.

The rate coefficients for these reactions as well as other parameters that were included in the model are summarized in Table 1. It should be noted that most published Cu-doped experiments have been performed in ammonium sulphate particles, where sulphate concentrations are expected to be greater than 3 M for all relative humidities that have been investigated.[27,31,39,40,42,43] Such high sulphate concentrations may cause Cu^{2+} to form a $CuSO_4$ complex, following a published equilibrium constant for this complex formation of 230.[63,69] Accordingly, at >3 M sulphate, $CuSO_4$ concentrations should be significantly higher than Cu^{2+} concentrations. Thus, we assume that all Cu is present in the form of $CuSO_4$ in the model for ammonium sulphate particles and that $CuSO_4$ can participate in Fenton-like reactions (reaction (R13)). However, additional measurements are required to confirm that $CuSO_4$ is the dominant species in the Cu-doped ammonium sulphate particles modeled in this work and that the equilibrium constant of 230 is valid under the experimental conditions. For the high sulphate concentrations in the experiments, most Fe^{3+} should form the $Fe(SO_4)^+$ and $Fe(OH)^{2+}$ complexes.[63] Both complexes are reported to have the same rate coefficient for their reaction with O_2^- and, for simplicity, the rate coefficient for the reaction of $Fe(SO_4)^+$ with HO_2 is used.[63,66] Sensitivity studies indicate that using the higher rate coefficient of $k_{BR,14} = 2.2 \times 10^{-16}$ cm^3 s^{-1} for the reaction of $Fe(OH)^{2+}$ with HO_2 makes a negligible difference for the simulations performed in this work.[63] Other parameters in Table 1 include the Henry's law constants of HO_2 and H_2O_2 (H_{HO_2} and $H_{H_2O_2}$, respectively), the bulk diffusion coefficient of all species (D_b), the desorption lifetime of HO_2 and H_2O_2 (τ_d), the surface accommodation coefficient of HO_2 and H_2O_2 onto an adsorbate-free surface ($\alpha_{s,0}$), the gas-phase diffusion coefficient of HO_2 and H_2O_2 (D_g), and the radius (r_p) and pH of the aerosol particles. Although the model is only applied to liquid particles in this work, it has the potential to be used for solid particles in the future by setting the partitioning coefficient into the bulk to zero. Transition metal

concentrations in Cu or Fe doped ammonium nitrate or ammonium sulphate particles were calculated using the following equation:

$$[\text{Cu}] \text{ or } [\text{Fe}] \text{ in the particles} = \frac{[\text{AN or AS}]\text{in the particles} \times [\text{Cu}] \text{ or } [\text{Fe}] \text{ in the atomizer}}{[\text{AN or AS}] \text{ in the atomizer}} \quad \text{(E9)}$$

The concentration of ammonium nitrate (AN) or ammonium sulphate (AS) in the particles was calculated for the flow tube relative humidity and temperature using the E-AIM.[58–60] For simplicity we have not included activity coefficients in the model, but it is worth noting that their inclusion has the potential to decrease uptake coefficients. Concentrations were approximately 180 times higher in the particles than in the atomizer solutions.

KM-SUB outputs two different uptake coefficients. The true uptake coefficient (γ_{HO_2}) is calculated using the near surface gas-phase concentration of a HO_2 molecule, whereas the effective uptake coefficient ($\gamma_{HO_{2,eff}}$) is calculated using the (far-surface) gas-phase concentration to derive the collision flux of HO_2 onto the particle surface.[62] Hence, $\gamma_{HO_{2,eff}}$ implicitly considers gas-diffusion effects and is typically the observable in measurements and an important variable in atmospheric models when no other form of gas-diffusion correction is performed. The near surface-gas phase concentration can be significantly smaller than the gas-phase concentration if there are gas-diffusion limitations, which can be the case for large particles and fast uptake.[62] For most of the modelling performed in this work, the differences between γ_{HO_2} and $\gamma_{HO_{2,eff}}$ were negligible and we only report γ_{HO_2} for simplicity. In sensitivity tests that used large particles, a difference was observed and separate values for γ_{HO_2} and $\gamma_{HO_{2,eff}}$ reported (see the Results section).

3. Results

3.1. Temperature-dependent experiments of γ_{HO_2}

The HO_2 uptake coefficients as a function of temperature are summarized in Table 2, which also provides more information about the specific conditions of the experiments.

Several studies have measured markedly different HO_2 uptake coefficients onto solid ammonium sulfate surfaces compared to sodium chloride surfaces, which is indicative of different surface interactions with HO_2.[38,40,52] It is therefore important to make measurements for both compounds which are commonly found in atmospheric particles. For deliquesced aerosol particles, ammonium nitrate (AN) aerosol particles were chosen because they do not effloresce down to humidities of 0% and therefore a correction could be made for their surface area between the flow tube and the DMA (as described in Section 2.4), which will exhibit different relative humidities. Fig. 2(a) shows an example of the pseudo-first order rate coefficients for loss of HO_2, k', onto deliquesced ammonium nitrate aerosol particles as a function of aerosol particle surface area for the two temperatures, at 263 K (RH = 53%, $[HO_2]_0 = 2.8 \times 10^8$ cm^{-3}) and at 312 K (RH = 18%, $[HO_2]_0 = 4.7 \times 10^8$ cm^{-3}). Fig. 2(b) shows measurements of γ_{HO_2} as a function of temperature for deliquesced ammonium nitrate and effloresced ammonium sulphate and sodium chloride aerosol particles.

The γ_{HO_2} measurements shown in Fig. 2 and summarized in Table 2, are the first measurements of γ_{HO_2} for suspended

Table 2 A summary of γ_{HO_2} measured using an atmospheric pressure aerosol flow tube over a range of temperatures. The 'moving injector' data analysis methodology was used (see Section 2.2)

Temperature/K	Aerosol particle type	Effloresced or deliquesced	Relative humidity/%	Initial HO_2 concentration/10^8 cm^{-3}	γ_{HO_2}
314	Sodium chloride	Effloresced	9	8.9	0.004 ± 0.002
304		Effloresced	25	6.6	0.002 ± 0.003
292		Effloresced	36	9.8	0.004 ± 0.003
284		Effloresced	39	17	0.001 ± 0.002
274		Effloresced	57	6.0	0.001 ± 0.002
263		Effloresced	40	5.3	0.000 ± 0.002
314	Ammonium sulphate	Effloresced	10	10	0.002 ± 0.003
304		Effloresced	13	12	0.003 ± 0.002
292		Effloresced	21	6.9	0.001 ± 0.002
284		Effloresced	39	8.0	0.001 ± 0.001
274		Effloresced	67	2.4	0.000 ± 0.002
263		Effloresced	46	3.0	0.000 ± 0.001
292	Copper doped ammonium nitrate	Deliquesced	33	12	0.62 ± 0.05
284		Deliquesced	33	13	0.71 ± 0.03
275		Deliquesced	42	9.7	0.65 ± 0.03
263		Deliquesced	43	6.1	0.71 ± 0.06
312	Ammonium nitrate	Deliquesced	18	4.7	0.005 ± 0.002
302		Deliquesced	36	9.7	0.007 ± 0.002
292		Deliquesced	45	13	0.005 ± 0.001
284		Deliquesced	50	12	0.007 ± 0.003
275		Deliquesced	52	6.1	0.010 ± 0.002
263		Deliquesced	53	3.8	0.016 ± 0.005

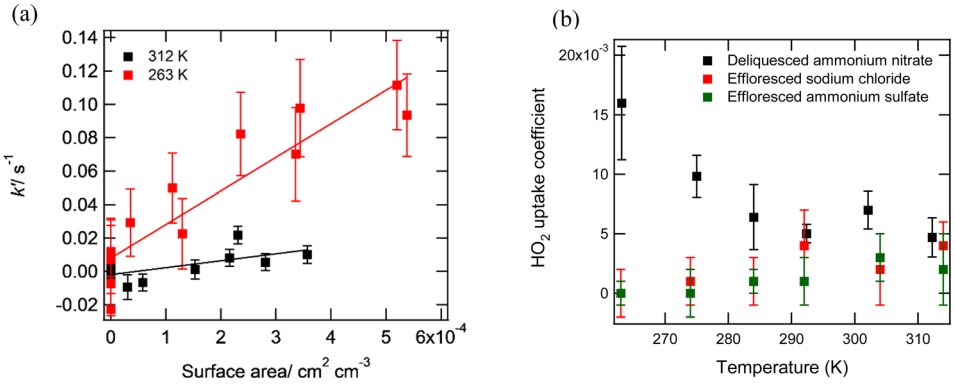

Fig. 2 Panel (a) k' as a function of the surface area per unit concentration of ammonium nitrate aerosol particles at two different temperatures (T = 312 K, RH = 18%, initial $[HO_2] = 4.7 \times 10^8$ cm^{-3}; T = 263 K, RH = 53%; initial $[HO_2] = 3.8 \times 10^8$ cm^{-3}) and linear fits to experimental data; panel (b) measured γ_{HO_2} as a function of temperature for deliquesced ammonium nitrate, effloresced sodium chloride and effloresced ammonium sulphate aerosol particles. See Table 2 for conditions of these experiments. The errors represent two standard deviations of between 2 and 8 replicate experiments.

deliquesced or effloresced aerosol particles as a function of temperature. The γ_{HO_2} increases significantly as the temperature decreases for deliquesced ammonium nitrate particles, which is consistent with the trend in the work by Thornton *et al.*[47] Although the rate coefficients (R4) and (R5) are likely to increase with increasing temperatures, the Thornton *et al.*[47] model demonstrated that the effect of the Henry's law constant dominates over the rate coefficients to decrease γ_{HO_2} as the temperature increases. Therefore, with increasing temperature, the decrease in the γ_{HO_2} is the expected behaviour in deliquesced particles due to a smaller HO_2 concentration in the bulk of the aerosol particle and available for self-reaction.

Although there are currently no measured γ_{HO_2} onto aerosol particles over a range of temperatures reported in the literature, several different studies have measured γ_{HO_2} onto aqueous sulphuric acid surfaces at low temperatures and onto aqueous sulphuric acid aerosol particles at room temperature. The γ_{HO_2} was measured to be < 0.01 at 295 K,[39] > 0.05 at 249 K.[53] > 0.2 at 243 K (ref. 52) and 0.055 ± 0.020 at 223 K.[51] Overall, there appears to be an increase in γ_{HO_2} with decreasing temperature. However, no study has systematically measured γ_{HO_2} over a range of temperatures. Griffiths and Cox[70] measured N_2O_5 uptake coefficients between 263 and 303 K onto aqueous ammonium sulphate and aqueous ammonium bisulphate aerosol particles at a relative humidity of 50%. The uptake coefficients varied from 0.005 ± 0.002 at 303 K to 0.036 ± 0.002 at 263 K for ammonium sulphate and from 0.003 ± 0.001 at 303 K to 0.036 ± 0.009 at 263 K for ammonium bisulphate.

The copper(I and II) and iron(II and III) concentrations in the atomiser solutions for all experiments were measured using Inductively Coupled Plasma Mass Spectrometry (ICP-MS) and it was found that although all solutions did contain trace metal contamination, the concentrations were less than 5 ppb. The estimated copper(II) molarity in the aerosol particles was always less than 5×10^{-5} M for both copper(I and II) and iron(II and III) over the range of temperatures and humidities used. As shown in Section 3.3 below, the observed γ_{HO_2} should therefore not be affected by these levels of trace metals, and trace metals can be ruled out as an explanation for the difference between the measurements in this work and those predicted by the Thornton *et al.*[47] model. The limiting factors for HO_2 uptake into non-copper doped aqueous ammonium nitrate aerosol particles is likely therefore to be solubility and the rate of reaction of HO_2, both of which are temperature dependent.

As shown in Fig. 2(b) and Table 2, a slight increase in γ_{HO_2} with temperature is observed for the effloresced sodium chloride and ammonium sulphate particles, with γ_{HO_2} increasing from 0.000 ± 0.001 to 0.004 ± 0.003. However, some of the dependence may be due to a decrease in the relative humidity at higher temperatures (see Table 2 for details of experimental conditions), as it was not possible to keep the RH constant over the range of temperatures used as the flow tube and the DMA were at different temperatures. Measurements have previously shown that the presence of water vapor can block reactive sites on a solid surface and lead to a decrease in γ_{HO_2}.[71] Other factors, such as HO_2 concentration affecting the uptake measured for these experiments, are also possible. We return to the effect of HO_2 concentration in Section 3.2. below. In contrast to this work, Remorov *et al.*[71] and Loukhovitskaya *et al.*[72] observed a negative temperature dependence for HO_2 uptake to solid coatings of sodium chloride with larger γ_{HO_2} at lower temperatures. The mass accommodation (α_{HO_2}) is likely to be temperature dependent as will be discussed below for copper doped aerosol particles. Both Remorov *et al.*[71] and Loukhovitskaya *et al.*[72] worked at 0% RH. However, when Remorov *et al.*[71] increased the water vapour in their flow tube from $[H_2O]$ = 0 molecule per cm^3 to $[H_2O] = 3 \times 10^{15}$ molecule per cm^3 the uptake coefficient decreased by 13 and 21% at 295 K (RH ~0.5%) and 243 K (RH ~28%), respectively. Therefore, the lower γ_{HO_2} at lower temperatures observed in this work may be due to the higher relative humidities that were utilised, meaning that this work is not inconsistent with the work by Remorov *et al.*[71] and Loukhovitskaya *et al.*[72]

The mass accommodation coefficient, α_{HO_2}, onto aerosol particles is also expected to be dependent upon temperature. As for previous work, doping with aerosol particles with sufficient Cu(II) means that the uptake of HO_2 is not limited by aqueous chemistry, rather by mass accommodation, and hence

a measurement of γ_{HO_2} yields α_{HO_2}. Table 2 shows the results and also gives the conditions for measurements of the temperature dependence of the mass accommodation α_{HO_2} as a function of temperature for copper(II)-doped ammonium nitrate aerosol particles. The aerosol particle copper(II) concentration was estimated as ~0.7 M, for which the lifetime of HO_2 within the aerosol particle is around 100 nanoseconds. It shows that the mass accommodation increases very slightly from $\alpha_{HO_2} = 0.62 \pm 0.05$ to 0.71 ± 0.06 between 292 and 263 K which is consistent with known theory about the dynamics and kinetics of the gas–liquid interfaces. Bulk mass accommodation is expected to be temperature dependent following an Arrhenius-type relationship in which the Gibbs free energy barrier of the transition state between the gaseous and solvated phases, ΔG_{solv}, governs the temperature dependence of the process. ΔG_{solv} is usually negative for small molecules on aqueous solutions, hence leading to higher accommodation coefficients at lower temperatures.[73] This is in part due to the strong temperature dependence of desorption and reversible adsorption, respectively, which are central to interfacial transport and gas-particle exchange.[74]

Due to the variability in the conditions of the experiments (*e.g.* RH, wall loss and HO_2 concentration) and a large number of parameters (*e.g.* rate coefficients, Henry's law constants) required for the KM-SUB model where the temperature dependence is unknown, we did not attempt to calculate the temperature dependence of γ_{HO_2} with the model for comparison with experiments.

3.2. Dependence of γ_{HO_2} on reaction time and HO_2 concentration

Fig. 3 shows an example of the measured pseudo-first-order rate coefficient for the loss of HO_2, k', as a function of aerosol particle surface area for deliquesced sodium chloride aerosol particles at 59% RH and $T = 293$ K for different reaction times using the fixed injector methodology. From eqn (E2), the gradient is proportional to γ_{HO_2}, and it is evident from Fig. 3 that γ_{HO_2} decreases for larger reaction times.

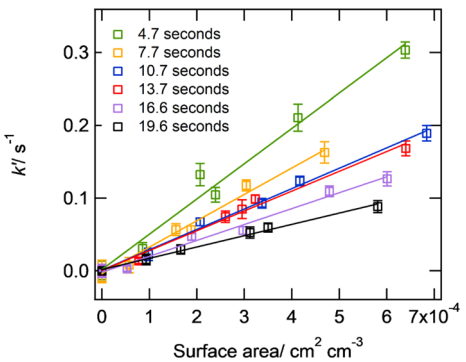

Fig. 3 k' as a function of the surface area per unit concentration of deliquesced sodium chloride aerosol particles at 59% RH and 293 ± 2 K, and for an initial HO_2 concentration at time zero of 2.1×10^9 molecule per cm^3 for a variety of reaction times (injector position varying from 20–70 cm along the flow-tube) using the 'fixed injector' methodology. The solid lines represent linear-least squares fits to the data (eqn (2)). The error bars represent one standard deviation.

Fig. 4(a) shows 'moving injector' measurements and modelling of the HO_2 uptake coefficient as a function of the initial flow tube HO_2 gas-phase concentration. The model predicts that γ_{HO_2} will increase with increasing HO_2 concentrations and should be proportional to $[HO_2]_g$ unless it becomes large enough to be limited by mass accommodation. This relationship has previously been described in Thornton *et al.*[47] and a brief explanation follows. The γ_{HO_2} can be calculated as the net adsorption flux divided by the collision flux. Unless limited by mass accommodation, the adsorption flux should be controlled by reaction and therefore it is proportional to $k_{BR,4}[HO_2]^2 + k_{BR,5}[HO_2][O_2^-]$. The collision flux is proportional to $[HO_2]_g$, resulting in γ_{HO_2} being proportional to $[HO_2]_g$. However, overall measurements collated from several studies do not appear to follow any trend and are quite scattered. Calculations performed using E-AIM suggest that $(NH_4)_2SO_4$ particles should have a pH $\leq$ 4. Measurements were significantly higher than those predicted using the model suggesting that perhaps the pH was higher than expected or that trace metal contamination played a role in increasing γ_{HO_2} which will be explored further in Fig. 4(c) below. The measurement by Thornton and Abbatt at a high $[HO_2]_g$ and with a particle buffered to pH = 5.1 was close to the modelled value. In contrast, most measurements with NaCl particles were smaller than the expected γ_{HO_2} for particles with a pH = 7, which may be partly due to the HO_2 concentrations along the flow tube being lower than the initial HO_2 concentration due to wall loss, gas-phase reactions, and uptake to particles. Changes in $[HO_2]_g$ were not considered in the modelling of this figure and will be explored below.

Fig. 4(b–d) show examples of γ_{HO_2} time dependence which were measured using the 'fixed injector' methodology for different aerosol particle compositions and conditions. For all examples, γ_{HO_2} decreases as a function of time. The kinetic model predicts this behaviour for particles that do not contain transition metals (Fig. 4(b and c)) and is able to reproduce the measured trends and the measurements within a factor of two for uptake to NaCl particles by accounting for HO_2 loss along the flow tube. Gas-phase reactions, wall losses and uptake to particles account for 1–4%, 10–79% and 17–89% of the total HO_2 loss, respectively, for the simulations shown in Fig. 4(b). Lower HO_2 concentrations lead to lower uptake coefficients in the absence of metals as γ_{HO_2} is controlled by the aqueous self-reactions of HO_2 (reactions (R4) and (R5)) as discussed above.

The kinetic model predicts that γ_{HO_2} would be higher if the initial HO_2 concentration is higher, but the opposite trend is observed in measurements (Fig. 4(b)). Although the reason for the trend in the measurements remains uncertain, model sensitivity tests indicate that there are many factors that could influence the HO_2 concentration along the flow tube and could potentially skew the uptake coefficient at a given time. For example, variability between experiments such as larger wall losses and higher particle concentrations can cause a reduction in the HO_2 concentration and uptake coefficient. The kinetic model indicated that changing the concentration of the

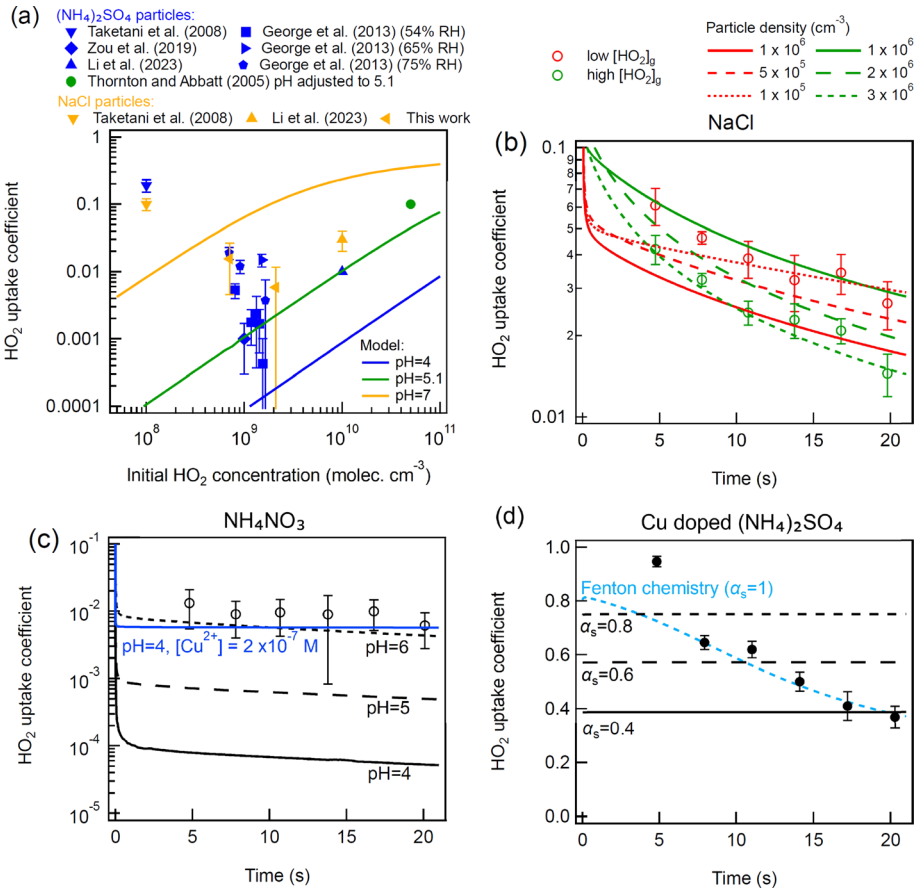

Fig. 4 Panel (a): measurements (markers) and modelling (lines) of γ_{HO_2} as a function of HO_2 concentration and pH for $(NH_4)_2SO_4$ particles and NaCl particles. Measurements were performed using the 'moving injector' methodology. Panels (b–d): measurements (markers) and kinetic modelling (lines) of γ_{HO_2} as a function of time using the 'fixed injector' methodology. Experiments in panel (a) were performed with NaCl particles and initial HO_2 concentrations of 2.1×10^9 cm^{-3} (green) and 7.1×10^8 cm^{-3} (red). The experiment in panel (c) was conducted with NH_4NO_3 particles and an initial HO_2 concentration of 1×10^9 cm^{-3}. The experiment in panel (d) was conducted using Cu doped $(NH_4)_2SO_4$ particles and an initial HO_2 concentration of 2.7×10^9 cm^{-3}. NaCl particles are assumed to have a pH of 7 and Cu doped $(NH_4)_2SO_4$ particles are assumed to have a pH of 4. Model simulation parameters are shown in Table 1. Measurements in panel (d) have previously been shown in George *et al.*[38] (2013). In panel (a) a constant $[HO_2]_g$ is assumed, while in panels (b–d) HO_2 decreases along the flow tube. In panel (d) the black lines represent the modelled uptake coefficient in the absence of Fenton chemistry for particles containing $[Cu(SO_4)] = 0.6$ M while the dashed blue line assumes that Fenton-like chemistry is occurring with an initial H_2O_2 concentration of 2×10^{12} cm^{-3}, a particle number density of 10^5 cm^{-3} and a H_2O_2 uptake coefficient to the walls of 6.5×10^{-6}.

particles could lead to the trends observed during the measurements (Fig. 4(b)). Alternatively, it can be speculated that setting the lamp in the injector to a higher power to obtain higher initial HO_2 concentrations may lead to slightly higher initial temperatures resulting in a lower HO_2 partitioning coefficient and different initial mixing conditions. More H_2O_2 is also expected to exit the injector at higher HO_2 concentrations which could potentially be converted back to HO_2 by Fenton chemistry if there are trace transition metal contaminants in the particles, thereby effectively reducing γ_{HO_2}. Note that although the ICP-MS measurements indicated low metal contamination, any contamination would become enhanced in the concentrated particles, and we cannot fully disregard contamination from impacting γ_{HO_2}. However, the cause of the measured HO_2 concentration dependence remains uncertain and warrants further investigation in the future.

Fig. 4(c) shows time dependent measurements of γ_{HO_2} for ammonium nitrate particles. The overall trend in the uptake coefficients as a function of time is similar to NaCl particles but γ_{HO_2} are significantly smaller. Ammonium nitrate aerosol particles have a lower pH than NaCl aerosol particles which causes the slower reaction (R4) to become more important compared to reaction (R5) and leads to less overall partitioning of HO_2 into the particles (reaction (R3)). Calculations performed with the E-AIM model suggest that the pH of the ammonium nitrate particles should have been <4.[58–60] However, with a pH of 4 the model underestimates γ_{HO_2} measurements significantly. Further sensitivity tests indicated that the measurements could be reproduced if contaminants increased the pH to 6 or if there was a small amount of transition metal contamination (*e.g.* $[Cu^{2+}] \sim 2 \times 10^{-7}$ M) which could be consistent with ICP-MS measurements. Note that uncertainty remains with regards to the formation of Cu complexes in ammonium nitrate particles

and free Cu ion rate coefficients have been assumed for this simulation.

Fig. 4(d) shows an example of the significant time dependence of γ_{HO_2} for copper-doped ammonium sulphate particles. For these particles, the kinetic model predicts that there should be no time dependence in the experiments and that γ_{HO_2} should be approximately the same as the surface mass accommodation coefficient (Fig. 4(d)). This discrepancy between the model and the measurements could be due to and influenced by a variety of factors. Firstly, we cannot exclude the possibility that uneven mixing in the initial part of the flow tube, in the region before laminar flow is achieved, could be causing the measured initial high uptake coefficients. An alternative explanation that has been explored with the model is that Fenton-like chemistry may be occurring. H_2O_2 is formed in the injector from the self-reaction of HO_2. As the ratio of $HO_2 : H_2O_2$ decreases along the flow tube, HO_2 formation from Fenton-like chemistry becomes more important and the uptake coefficient decreases. Sensitivity tests indicated that the measurements were able to be reproduced well by assuming an initial H_2O_2 concentration of 2.5×10^{12} cm^{-3}, a particle number density of 10^5 cm^{-3} and a H_2O_2 uptake coefficient to the walls of 6.5×10^{-6} (same value as for HO_2) (Fig. 4(d)). However, further measurements and more complex modelling are required to better understand these trends and to determine whether Fenton-like chemistry is important in these experiments. It should also be noted that an assumption has been made that $CuSO_4$ reacts with H_2O_2 in a similar way and with the same rate coefficient as Cu^{2+} reacting with H_2O_2. A different rate coefficient would impact the H_2O_2 concentration required to fit the measurements. Guo *et al.*[30] determined the impact of the aqueous production of HO_2 on the uptake coefficient. They concluded that the aqueous-phase production of HO_2 is an important factor that influences γ_{HO_2}. However, they did not elaborate which reactions exactly could be responsible for such production. In this work, we are proposing Fenton and Fenton-like chemistry as a possible route, at least in the experimental conditions, to explain this reformation of HO_2.

3.3. Dependence of γ_{HO_2} on the Cu and Fe concentration

Fig. 5(a) and (b) show measurements from different studies of γ_{HO_2} as a function of Cu and Fe concentrations, respectively, as well as kinetic modelling results. The kinetic model can fit the measurements for Cu doped aerosol particles relatively well with literature rate coefficients if we assume that all Cu is present as $CuSO_4$. The slower rate coefficients of $CuSO_4$ with HO_2/O_2^- compared to Cu^{2+} with HO_2/O_2^- assumed in this work lead to lower γ_{HO_2} than if free Cu^{2+} ions were present in the particles (brown line, Fig. 5(a)). Note that for the free Cu^{2+} simulation, γ_{HO_2} is mainly controlled by the fast reactions of $Cu^{2+} + O_2^-$ and $Cu^+ + HO_2/O_2^-$ and that decreasing the rate coefficient of $Cu^{2+} + HO_2$ has a negligible impact on γ_{HO_2} at pH = 4. It is necessary to vary the surface accommodation coefficient to obtain a good fit to different datasets (Fig. 5(a)). The varying measured mass accommodation coefficients are most likely an experimental artefact which may be due to mixing conditions, Fenton-like chemistry (as discussed above), activity coefficients (which are not treated in the model) or some other currently unknown process or reaction. A trend in the uptake coefficient onto Cu-doped aerosol particles as a function of relative humidity has been previously described although the reasons for this remain unclear.[42] It should be noted that the Song *et al.*[27] measurements, which the model does not reproduce, are performed at the lowest relative humidity of the different studies (~43% RH). The model overestimates the uptake coefficient for Fe-doped particles (Fig. 5(b)), which may be due to Fe precipitation. Significant precipitation of iron was observed in the atomizer solutions one day after they were prepared in this work, which could also be occurring in the concentrated aerosol particles reducing its availability for reaction. Although the chemical formula of the precipitate has not been ascertained, it could be $Fe(OH)_2$ or $Fe(OH)_3$. Trace organics have also been shown to have the potential to reduce γ_{HO_2} onto Cu-doped aerosol particles.[43] Note that sensitivity tests indicate that for atmospherically relevant copper concentrations, the uptake coefficient is independent of $[HO_2]_g$ when $[HO_2]_g$ is less than 1×10^{11} cm^{-3}.

Fig. 5(c) and (d) show the same experimental measurements but with kinetic modelling pH sensitivity test results for atmospherically relevant aerosol particle pH values. Fitting results to measurements indicate that aerosol particles used in the experimental measurements are most likely to exhibit a pH $\leq$ 4, which is consistent with ammonium sulphate particles doped with copper and is also consistent with previous modelling work.[27,31] Increasing the pH leads to higher uptake coefficients as the HO_2 dissociates to form O_2^- and the effective partitioning coefficient into the particles increases. Changes in pH also lead to a change in the O_2^- to HO_2 ratio resulting in a different overall rate of destruction (reactions (R6), (R7), (R14) and (R15)). However, decreasing the pH below 3 has a negligible effect for Cu-doped particles as HO_2, which has a pK_a of 4.7, is already almost entirely protonated and reaction (R6) dominates over reaction (R7).[26] For the equivalent Fe reactions, there is a much larger difference between $k_{BR,14}$ and $k_{BR,15}$ leading to reaction (R15) controlling the uptake even at a low pH of 3.

The blue shaded area in Fig. 5 represents a typical range of total soluble iron and copper concentrations measured in different locations and cities in $PM_{2.5}$ (Fe: 0.003–1.5% soluble mass fraction, Cu: 0.0008–0.11% soluble mass fraction[75]). For aerosol particles with a 50 nm radius shown in Fig. 5(c and d), γ_{HO_2} can be equal to a wide range of values in these Cu and Fe concentration ranges, depending on the actual soluble transition metal concentration and the pH. Note that the soluble Cu and Fe concentrations may be different for these smaller particles, but far fewer measurements exist compared to $PM_{2.5}$.[76–78] As of now measurements have been performed on ammonium sulphate particles but future measurements of γ_{HO_2} as a function of Cu and Fe concentrations should be performed for a wide range of particle compositions for the best comparison with atmospherically relevant concentrations and to gain a better understanding of how the particle composition can influence measurements. It should also be noted that the reaction of $Cu^+ + O_2 \rightarrow Cu^{2+} + O_2^-$ has not been included in the model simulations as many

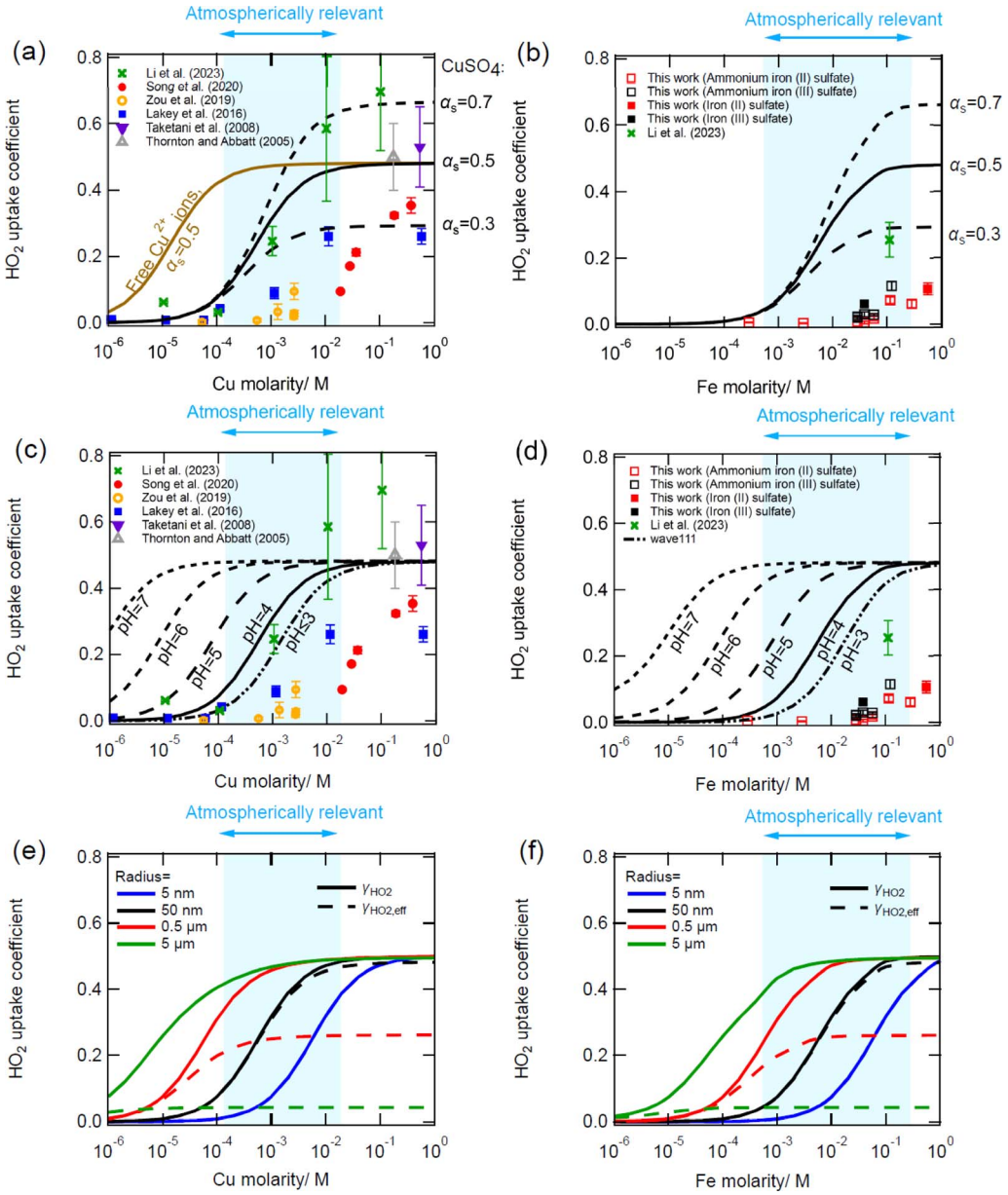

Fig. 5 Measurements (markers) and modelling (lines) of γ_{HO_2} as a function of (a, c and e) Cu molarity and (b, d and f) Fe molarity in AS particles. Fe experiments in this work were performed at 293 ± 2 K and 66 ± 2% RH. Panels (a and b) show model sensitivity tests for different surface mass accommodations. Panels (c and d) show model sensitivity tests as a function of pH. Panels (e and f) show model sensitivity tests as a function of particle radius. Model simulations are run with a constant HO_2 concentration of 1×10^9 cm^{-3}, $\alpha_s = 0.5$, pH = 4 and with a particle radius of 50 nm unless otherwise stated. The atmospherically relevant molarities of soluble iron (5.4×10^{-4} –0.27 M) and copper (1.3×10^{-4}–0.018 M) in $PM_{2.5}$ particles are shown by the blue shaded area.

experiments were performed under nitrogen. Sensitivity studies indicate that the inclusion of this reaction with a rate coefficient of 7.6×10^{-16} cm^{-3} s^{-1} would lower the HO_2 uptake coefficient by approximately 16–18% when [Cu] $\leq 10^{-3}$ M for particles with pH = 4.[63,79] For higher Cu concentrations the reduction in the HO_2 uptake coefficient becomes smaller and with a concentration of 1 M the HO_2 uptake coefficient is only reduced by approximately 1%. Additional reactions could also be included in future versions of the model.[63]

Fig. 5(e–f) demonstrate the importance of aerosol particle size on γ_{HO_2}. As the aerosol particle radius increases, γ_{HO_2} (calculated with the near surface gas-phase HO_2 concentration) also increases due to larger volumes in which the reaction can occur for a given surface area. However, the effective γ_{HO_2} (calculated with the HO_2 gas-phase concentration), which includes gas-phase diffusion limitations, is likely to be significantly reduced. For example, for 5 μm particles the effective uptake coefficient is predicted to be ~0.04 over the atmospherically relevant Cu concentration range. This is consistent with a low Knudsen number of 0.034 for this particle radius, which according to gas-kinetic theory will cause a decrease in the near-surface gas concentration, leading to a significant decrease in the effective

uptake coefficient in the atmospherically relevant range of transition metal concentrations.[62] It should also be noted that for the simulations discussed above, no bulk diffusion limitations due to viscous particles or metal complexation is treated, but these factors have previously been studied and shown to have the potential to reduce γ_{HO_2} significantly for particles containing high transition metal concentrations.[43,54]

4. Discussion and outlook

Our measurements suggest that temperature has a large impact on γ_{HO_2}, which is consistent with previous parameterizations and known theoretical frameworks.[15,73] However, we are currently unable to constrain these measurements with our KM-SUB model due to the large number of uncertainties including the effect of temperature on the rate coefficients and Henry's law constants.

The KM-SUB model has demonstrated that a time dependence of γ_{HO_2} is expected in flow tube experiments for particles that do not contain transition metal ions. The γ_{HO_2} is controlled by HO_2 self-reaction in the aerosol particles and therefore decreases along the flow tube as $[HO_2]_g$ decreases. High wall losses and high particle concentrations can cause γ_{HO_2} to decrease significantly as a function of reaction time, which should be acknowledged when analysing HO_2 uptake measurement data in the future. This time dependence may increase with increasing RH, as wall losses and gas-phase reaction rate coefficients increase leading to lower HO_2 concentrations along the flow tube.[80] To obtain accurate γ_{HO_2} values it is necessary to use a model which accounts for decreasing HO_2 concentrations along the flow tube.

The value of γ_{HO_2} onto particles containing transition metal ions also has the potential to be time dependent in experiments if Fenton-like chemistry is occurring. HO_2 reformation from H_2O_2 would decrease the observed γ_{HO_2} as the $HO_2 : H_2O_2$ ratio decreases along the flow tube. Further but challenging experiments in which H_2O_2 concentrations are also measured would be required to confirm this. Gas-phase species such as H_2O_2, which partitions into aerosol particles in the aerosol flow tube and subsequently facilitates the formation of HO_2, have the capacity to elucidate variations observed in the scientific literature concerning diverse laboratory assessments of γ_{HO_2} onto Cu-doped particles. There may also be trace organic impurities in the gases or water used in the experiments which decompose in the presence of metal ions forming HO_2. Further investigations are required to determine whether any other species exist within the flow tube in addition to H_2O_2, that would form HO_2 or O_2^- within the particle phase. For example, it is known that the trace O_2 concentrations within the aerosol flow tube could react with trace iron and copper concentrations within the aerosol particles forming O_2^-.[64,65] Alternatively, HO_2 radicals could be formed from other mechanisms; for example, trace levels of O_3 reacting with H_2O_2 can lead to the formation of radicals.[81] The presence of gas-phase species which reform HO_2 in the atmosphere may lead to a decrease in the effective γ_{HO_2}. Further systematic measurements with known H_2O_2 and transition metal ions will be required to better understand the impact of ambient H_2O_2 concentrations in the atmosphere on the effective γ_{HO_2}.

The KM-SUB model was able to reproduce measurements of the γ_{HO_2} as a function of Cu relatively well with parameters consistent with previous work.[31] We speculate that the formation of $CuSO_4$ may significantly reduce γ_{HO_2} in ammonium sulphate particles although this still needs to be further investigated. We demonstrate that increasing aerosol particle pH can significantly increase the uptake coefficient γ_{HO_2} of aerosol particles containing transition metal ions due to additional partitioning of HO_2 into the particles and changes in the relative importance of different reactions. We have also demonstrated that although γ_{HO_2} will increase for larger particles, the effective uptake coefficient $\gamma_{HO_2,eff}$, which includes gas-phase diffusion limitations, will decrease significantly. This may lead to $\gamma_{HO_2,eff}$, which is the typical observable in experiments and parameter in atmospheric model simulations, being larger for smaller particles in the atmosphere.

It has been demonstrated that the value of γ_{HO_2} may vary significantly over the range of atmospherically relevant transition metal concentrations. This is consistent with previous measurements and modelling work.[27,30–33,35,82] Many factors may influence the value of γ_{HO_2} that should be used in atmospheric box models, such as the concentration of soluble transition metal ions, the particle composition, the pH, the aerosol particle size, and the presence of any compounds which reform HO_2. Other factors, such as bulk diffusion limitations or the presence of certain organics, can reduce γ_{HO_2}. As discussed in our previous work, an increase in aerosol particle viscosity can lead to a significant decrease in γ_{HO_2} for copper doped aerosol particles by decreasing the rate of diffusion of HO_2 into the aerosol particles.[54] We have also previously observed a significant decrease in γ_{HO_2} from a value of the mass accommodation coefficient α_{HO_2} to approximately two orders of magnitude less when oxalic acid is added to copper-doped aerosol particles.[43] In the current work we have not treated the interactions of Cu and Fe in aerosols, which may enhance HO_2 uptake, prevent iron precipitation in ambient aerosols, and should be investigated in follow-up studies.[63,83] Transition metal distribution across all particles is usually assumed to be even by models. However, in reality, not all atmospheric particles contain transition metals that catalytically remove HO_2 and enhance the value of γ_{HO_2}. This was discussed in a recent study in which Khaled *et al.*[84] hypothesise that γ_{HO_2} may be significantly lower for an atmospheric aerosol particle compared to an aerosol particle generated *via* atomisation in the laboratory using a bulk sample containing transition metal ions. Overall, additional experiments and modelling are required to fully understand the influence of different factors on the HO_2 uptake coefficient.

Conflicts of interest

There are no conflicts of interest to declare.

Acknowledgements

PSJL is grateful to the Natural Environmental Research Council (NERC) for the award of a studentship. DEH is grateful to the NERC for financial support *via* grant number NE/F020651/1. We

are grateful to Ingrid George, Lisa Whalley and Trevor Ingham for technical assistance, and to Professor Jonathan Abbatt for useful discussions.

References

1 D. Fowler, K. Pilegaard, M. Sutton, P. Ambus, M. Raivonen, J. Duyzer, D. Simpson, H. Fagerli, S. Fuzzi and J. K. Schjørring, Atmospheric composition change: ecosystems–atmosphere interactions, *Atmos. Environ.*, 2009, **43**, 5193–5267.

2 U. Pöschl and M. Shiraiwa, Multiphase Chemistry at the Atmosphere–Biosphere Interface Influencing Climate and Public Health in the Anthropocene, *Chem. Rev.*, 2015, **115**, 4440–4475.

3 R. A. Cox, M. Ammann, J. N. Crowley, H. Herrmann, M. E. Jenkin, V. F. McNeill, A. Mellouki, J. Troe and T. J. Wallington, Evaluated kinetic and photochemical data for atmospheric chemistry: Volume VII – Criegee intermediates, *Atmos. Chem. Phys.*, 2020, **20**, 13497–13519.

4 A. Mellouki, M. Ammann, R. A. Cox, J. N. Crowley, H. Herrmann, M. E. Jenkin, V. F. McNeill, J. Troe and T. J. Wallington, Evaluated kinetic and photochemical data for atmospheric chemistry: volume VIII – gas-phase reactions of organic species with four, or more, carbon atoms ($\geq C_4$), *Atmos. Chem. Phys.*, 2021, **21**, 4797–4808.

5 J. Burkholder, S. Sander, J. Abbatt, J. Barker, C. Cappa, J. Crounse, T. Dibble, R. Huie, C. Kolb and M. Kurylo, *Chemical Kinetics and Photochemical Data for Use in Atmospheric Studies; Evaluation Number 19*, Jet Propulsion Laboratory, National Aeronautics and Space, Pasadena, CA, 2020.

6 M. Ammann, R. A. Cox, J. Crowley, M. E. Jenkin, A. Mellouki, M. J. Rossi, J. Troe and T. J. Wallington, Evaluated kinetic and photochemical data for atmospheric chemistry: Volume VI–heterogeneous reactions with liquid substrates, *Atmos. Chem. Phys.*, 2013, **13**, 8045–8228.

7 W. H. Brune, D. Tan, I. F. Faloona, L. Jaegle, D. J. Jacob, B. G. Heikes, J. Snow, Y. Kondo, R. Shetter, G. W. Sachse, B. Anderson, G. L. Gregory, S. Vay, H. B. Singh, D. D. Davis, J. H. Crawford and D. R. Blake, OH and HO_2 chemistry in the North Atlantic free troposphere, *Geophys. Res. Lett.*, 1999, **26**, 3077–3080.

8 C. A. Cantrell, R. E. Shetter, T. M. Gilpin and J. G. Calvert, Peroxy radicals measured during Mauna Loa observatory photochemistry experiment 2: The data and first analysis, *J. Geophys. Res.: Atmos.*, 1996, **101**, 14643–14652.

9 N. Carslaw, D. J. Creasey, D. E. Heard, P. J. Jacobs, J. D. Lee, A. C. Lewis, J. B. McQuaid, M. J. Pilling, S. Bauguitte, S. A. Penkett, P. S. Monks and G. Salisbury, Eastern Atlantic Spring Experiment 1997 (EASE97) - 2. Comparisons of model concentrations of OH, HO_2, and RO_2 with measurements, *J. Geophys. Res.: Atmos.*, 2002, **107**, ACH 5.

10 N. Carslaw, D. J. Creasey, D. E. Heard, A. C. Lewis, J. B. McQuaid, M. J. Pilling, P. S. Monks, B. J. Bandy and S. A. Penkett, Modeling OH, HO_2, and RO_2 radicals in the marine boundary layer - 1. Model construction and comparison with field measurements, *J. Geophys. Res.: Atmos.*, 1999, **104**, 30241–30255.

11 A. L. Haggerstone, L. J. Carpenter, N. Carslaw and G. McFiggans, Improved model predictions of HO_2 with gas to particle mass transfer rates calculated using aerosol number size distributions, *J. Geophys. Res.: Atmos.*, 2005, **110**, D04304.

12 L. Jaegle, D. J. Jacob, W. H. Brune, I. Faloona, D. Tan, B. G. Heikes, Y. Kondo, G. W. Sachse, B. Anderson, G. L. Gregory, H. B. Singh, R. Pueschel, G. Ferry, D. R. Blake and R. E. Shetter, Photochemistry of HO_x in the upper troposphere at northern midlatitudes, *J. Geophys. Res.: Atmos.*, 2000, **105**, 3877–3892.

13 Y. Kanaya, R. Cao, S. Kato, Y. Miyakawa, Y. Kajii, H. Tanimoto, Y. Yokouchi, M. Mochida, K. Kawamura and H. Akimoto, Chemistry of OH and HO_2 radicals observed at Rishiri Island, Japan, in September 2003: Missing daytime sink of HO_2 and positive nighttime correlations with monoterpenes, *J. Geophys. Res.: Atmos.*, 2007, **112**, D11308.

14 Y. Kanaya, Y. Sadanaga, J. Matsumoto, U. K. Sharma, J. Hirokawa, Y. Kajii and H. Akimoto, Daytime HO_2 concentrations at Oki Island, Japan, in summer 1998: Comparison between measurement and theory, *J. Geophys. Res.: Atmos.*, 2000, **105**, 24205–24222.

15 J. Mao, D. J. Jacob, M. J. Evans, J. R. Olson, X. Ren, W. H. Brune, J. M. St Clair, J. D. Crounse, K. M. Spencer, M. R. Beaver, P. O. Wennberg, M. J. Cubison, J. L. Jimenez, A. Fried, P. Weibring, J. G. Walega, S. R. Hall, A. J. Weinheimer, R. C. Cohen, G. Chen, J. H. Crawford, C. McNaughton, A. D. Clarke, L. Jaegle, J. A. Fisher, R. M. Yantosca, P. Le Sager and C. Carouge, Chemistry of hydrogen oxide radicals (HO_x) in the Arctic troposphere in spring, *Atmos. Chem. Phys.*, 2010, **10**, 5823–5838.

16 S. C. Smith, J. D. Lee, W. J. Bloss, G. P. Johnson, T. Ingham and D. E. Heard, Concentrations of OH and HO_2 radicals during NAMBLEX: measurements and steady state analysis, *Atmos. Chem. Phys.*, 2006, **6**, 1435–1453.

17 R. Sommariva, W. J. Bloss, N. Brough, N. Carslaw, M. Flynn, A. L. Haggerstone, D. E. Heard, J. R. Hopkins, J. D. Lee, A. C. Lewis, G. McFiggans, P. S. Monks, S. A. Penkett, M. J. Pilling, J. M. C. Plane, K. A. Read, A. Saiz-Lopez, A. R. Rickard and P. I. Williams, OH and HO_2 chemistry during NAMBLEX: roles of oxygenates, halogen oxides and heterogeneous uptake, *Atmos. Chem. Phys.*, 2006, **6**, 1135–1153.

18 R. Sommariva, A. L. Haggerstone, L. J. Carpenter, N. Carslaw, D. J. Creasey, D. E. Heard, J. D. Lee, A. C. Lewis, M. J. Pilling and J. Zador, OH and HO_2 chemistry in clean marine air during SOAPEX-2, *Atmos. Chem. Phys.*, 2004, **4**, 839–856.

19 P. S. Stevens, J. H. Mather and W. H. Brune, Measurement of tropospheric OH and HO_2 by Laser Induced Fluorescence at low pressure, *J. Geophys. Res.: Atmos.*, 1994, **99**, 3543–3557.

20 D. Stone, L. K. Whalley and D. E. Heard, Tropospheric OH and HO_2 radicals: field measurements and model comparisons, *Chem. Soc. Rev.*, 2012, **41**, 6348–6404.

21 L. K. Whalley, K. L. Furneaux, A. Goddard, J. D. Lee, A. Mahajan, H. Oetjen, K. A. Read, N. Kaaden, L. J. Carpenter, A. C. Lewis, J. M. C. Plane, E. S. Saltzman, A. Wiedensohler and D. E. Heard, The chemistry of OH and HO_2 radicals in the boundary layer over the tropical Atlantic Ocean, *Atmos. Chem. Phys.*, 2010, **10**, 1555–1576.

22 J. R. Olson, J. H. Crawford, W. Brune, J. Mao, X. Ren, A. Fried, B. Anderson, E. Apel, M. Beaver, D. Blake, G. Chen, J. Crounse, J. Dibb, G. Diskin, S. R. Hall, L. G. Huey, D. Knapp, D. Richter, D. Riemer, J. S. Clair, K. Ullmann, J. Walega, P. Weibring, A. Weinheimer, P. Wennberg and A. Wisthaler, An analysis of fast photochemistry over high northern latitudes during spring and summer using in-situ observations from ARCTAS and TOPSE, *Atmos. Chem. Phys.*, 2012, **12**, 6799–6825.

23 M. de Reus, H. Fischer, R. Sander, V. Gros, R. Kormann, G. Salisbury, R. Van Dingenen, J. Williams, M. Zöllner and J. Lelieveld, Observations and model calculations of trace gas scavenging in a dense Saharan dust plume during MINATROC, *Atmos. Chem. Phys.*, 2005, **5**, 1787–1803.

24 H. Macintyre and M. Evans, Parameterisation and impact of aerosol uptake of HO_2 on a global tropospheric model, *Atmos. Chem. Phys.*, 2011, **11**, 10965–10974.

25 K. Li, D. J. Jacob, H. Liao, L. Shen, Q. Zhang and K. H. Bates, Anthropogenic drivers of 2013–2017 trends in summer surface ozone in China, *Proc. Natl. Acad. Sci. U. S. A.*, 2019, **116**, 422–427.

26 D. J. Jacob, Heterogeneous chemistry and tropospheric ozone, *Atmos. Environ.*, 2000, **34**, 2131–2159.

27 H. Song, X. Chen, K. Lu, Q. Zou, Z. Tan, H. Fuchs, A. Wiedensohler, D. R. Moon, D. E. Heard and M.-T. Baeza-Romero, Influence of aerosol copper on HO_2 uptake: a novel parameterized equation, *Atmos. Chem. Phys.*, 2020, **20**, 15835–15850.

28 H. Song, K. Lu, H. Dong, Z. Tan, S. Chen, L. Zeng and Y. Zhang, Reduced Aerosol Uptake of Hydroperoxyl Radical May Increase the Sensitivity of Ozone Production to Volatile Organic Compounds, *Environ. Sci. Technol. Lett.*, 2022, **9**, 22–29.

29 H. Fuchs, Z. Tan, K. Lu, B. Bohn, S. Broch, S. S. Brown, H. Dong, S. Gomm, R. Häseler, L. He, A. Hofzumahaus, F. Holland, X. Li, Y. Liu, S. Lu, K. E. Min, F. Rohrer, M. Shao, B. Wang, M. Wang, Y. Wu, L. Zeng, Y. Zhang and A. Wahner, OH reactivity at a rural site (Wangdu) in the North China Plain: contributions from OH reactants and experimental OH budget, *Atmos. Chem. Phys.*, 2017, **17**, 645–661.

30 J. Guo, Z. Wang, T. Wang and X. Zhang, Theoretical evaluation of different factors affecting the HO_2 uptake coefficient driven by aqueous-phase first-order loss reaction, *Sci. Total Environ.*, 2019, **683**, 146–153.

31 J. Li, Y. Sakamoto, K. Sato, Y. Morino and Y. Kajii, Investigation of HO_2 uptake onto Cu (II)-and Fe (II)-doped aqueous inorganic aerosols and seawater aerosols using laser spectroscopic techniques, *Environ. Sci.: Atmos.*, 2023, **3**, 1384–1395.

32 F. Taketani, Y. Kanaya, P. Pochanart, Y. Liu, J. Li, K. Okuzawa, K. Kawamura, Z. Wang and H. Akimoto, Measurement of overall uptake coefficients for HO_2 radicals by aerosol particles sampled from ambient air at Mts. Tai and Mang (China), *Atmos. Chem. Phys.*, 2012, **12**, 11907–11916.

33 J. Zhou, K. Murano, N. Kohno, Y. Sakamoto and Y. Kajii, Real-time quantification of the total HO_2 reactivity of ambient air and HO_2 uptake kinetics onto ambient aerosols in Kyoto (Japan), *Atmos. Environ.*, 2020, **223**, 117189.

34 J. Zhou, K. Sato, Y. Bai, Y. Fukusaki, Y. Kousa, S. Ramasamy, A. Takami, A. Yoshino, T. Nakayama, Y. Sadanaga, Y. Nakashima, J. Li, K. Murano, N. Kohno, Y. Sakamoto and Y. Kajii, Kinetics and impacting factors of HO2 uptake onto submicron atmospheric aerosols during the 2019 Air QUAlity Study (AQUAS) in Yokohama, Japan, *Atmos. Chem. Phys.*, 2021, **21**, 12243–12260.

35 J. Zhou, Y. Fukusaki, K. Murano, T. Gautam, Y. Bai, Y. Inomata, H. Komatsu, M. Takeda, B. Yuan and M. Shao, Investigation of HO_2 uptake mechanisms onto multiple-component ambient aerosols collected in summer and winter time in Yokohama, Japan, *J. Environ. Sci.*, 2024, **137**, 18–29.

36 P. D. Ivatt, M. J. Evans and A. C. Lewis, Suppression of surface ozone by an aerosol-inhibited photochemical ozone regime, *Nat. Geosci.*, 2022, **15**, 536–540.

37 P. S. J. Lakey, I. J. George, L. K. Whalley, M. T. Baeza-Romero and D. E. Heard, Measurements of the HO_2 Uptake Coefficients onto Single Component Organic Aerosols, *Environ. Sci. Technol.*, 2015, **49**, 4878–4885.

38 I. J. George, P. S. J. Matthews, L. K. Whalley, B. Brooks, A. Goddard, M. T. Baeza-Romero and D. E. Heard, Measurements of uptake coefficients for heterogeneous loss of HO_2 onto submicron inorganic salt aerosols, *Phys. Chem. Chem. Phys.*, 2013, **15**, 12829–12845.

39 J. Thornton and J. P. D. Abbatt, Measurements of HO_2 uptake to aqueous aerosol: Mass accommodation coefficients and net reactive loss, *J. Geophys. Res.: Atmos.*, 2005, **110**, D08309.

40 F. Taketani, Y. Kanaya and H. Akimoto, Kinetics of heterogeneous reactions of HO_2 radical at ambient concentration levels with $(NH_4)_2SO_4$ and NaCl aerosol particles, *J. Phys. Chem. A*, 2008, **112**, 2370–2377.

41 F. Taketani, Y. Kanaya and H. Akimoto, Kinetic Studies of Heterogeneous Reaction of HO_2 Radical by Dicarboxylic Acid Particles, *Int. J. Chem. Kinet.*, 2013, **45**, 560–565.

42 Q. Zou, H. Song, M. Tang and K. Lu, Measurements of HO_2 uptake coefficient on aqueous $(NH_4)_2SO_4$ aerosol using aerosol flow tube with LIF system, *Chin. Chem. Lett.*, 2019, **30**, 2236–2240.

43 P. S. J. Lakey, I. J. George, M. T. Baeza-Romero, L. K. Whalley and D. E. Heard, Organics substantially reduce HO_2 uptake onto aerosols containing transition metal ions, *J. Phys. Chem. A*, 2016, **120**, 1421–1430.

44 M. Mozurkewich, P. H. McMurry, A. Gupta and J. G. Calvert, Mass Accommodation Coefficient For HO_2 Radicals On

Aqueous Particles, *J. Geophys. Res.: Atmos.*, 1987, **92**, 4163–4170.

45 B. H. J. Bielski, D. E. Cabelli, R. L. Arudi and A. B. Ross, Reactivity of HO_2/O_2^- radicals in aqueous solution, *J. Phys. Chem. Ref. Data*, 1985, **14**, 1041–1100.

46 P. S. J. Matthews, M. T. Baeza-Romero, L. K. Whalley and D. E. Heard, Uptake of HO_2 radicals onto Arizona test dust particles using an aerosol flow tube, *Atmos. Chem. Phys.*, 2014, **14**, 7397–7408.

47 J. A. Thornton, L. Jaegle and V. F. McNeill, Assessing known pathways for HO_2 loss in aqueous atmospheric aerosols: Regional and global impacts on tropospheric oxidants, *J. Geophys. Res.: Atmos.*, 2008, **113**, D05303.

48 Y. M. Gershenzon, V. Grigorieva, A. Y. Zasypkin, A. Ivanov, R. Remorov and E. Aptekar, Capture of HO_2 radicals by an NH_4NO_3 surface at low temperatures, *Russ. J. Phys. Chem. B*, 1999, **18**, 79–90.

49 R. Remorov, Y. M. Gershenzon, L. Molina and M. Molina, Kinetics and mechanism of HO_2 uptake on solid NaCl, *J. Phys. Chem. A*, 2002, **106**, 4558–4565.

50 E. Loukhovitskaya, Y. Bedjanian, I. Morozov and G. Le Bras, Laboratory study of the interaction of HO_2 radicals with the NaCl, NaBr, $MgCl_2 \cdot 6H_2O$ and sea salt surfaces, *Phys. Chem. Chem. Phys.*, 2009, **11**, 7896–7905.

51 P. L. Cooper and J. P. D. Abbatt, Heterogeneous interactions of OH and HO_2 radicals with surfaces characteristic of atmospheric particulate matter, *J. Phys. Chem.*, 1996, **100**, 2249–2254.

52 Y. M. Gershenzon, V. M. Grigorieva, A. V. Ivanov and R. G. Remorov, O_3 and OH sensitivity to heterogeneous sinks of HO_x and CH_3O_2 on aerosol particles, *Faraday Discuss.*, 1995, **100**, 83–100.

53 D. R. Hanson, J. B. Burkholder, C. J. Howard and A. R. Ravishankara, Measurement Of OH And HO_2 Radical Uptake Coefficients On Water And Sulfuric-Acid Surfaces, *J. Phys. Chem.*, 1992, **96**, 4979–4985.

54 P. S. Lakey, T. Berkemeier, M. Krapf, J. Dommen, S. S. Steimer, L. K. Whalley, T. Ingham, M. T. Baeza-Romero, U. Pöschl and M. Shiraiwa, The effect of viscosity and diffusion on the HO_2 uptake by sucrose and secondary organic aerosol particles, *Atmos. Chem. Phys.*, 2016, **16**, 13035–13047.

55 D. E. Heard and M. J. Pilling, Measurement of OH and HO_2 in the troposphere, *Chem. Rev.*, 2003, **103**, 5163–5198.

56 R. L. Brown, Tubular Flow Reactors With 1st-Order Kinetics, *J. Res. Natl. Bur. Stand.*, 1978, **83**, 1–8.

57 N. A. Fuchs and A. G. Sutugin, *Properties of highly dispersed aerosols*, Ann Arbor Science Publishers, Ann Arbor, MI, 1970.

58 A. S. Wexler and S. L. Clegg, Atmospheric aerosol models for systems including the ions H^+, NH_4^+, Na^+, SO_4^{2-}, NO_3^-, Cl^-, Br^-, and H_2O, *J. Geophys. Res.: Atmos.*, 2002, **107**, ACH 14-11–ACH 14-14.

59 S. L. Clegg, K. S. Pitzer and P. Brimblecombe, Thermodynamics of multicomponent, miscible, ionic solutions. Mixtures including unsymmetrical electrolytes, *J. Phys. Chem.*, 1992, **96**, 9470–9479.

60 S. L. Clegg, P. Brimblecombe and A. S. Wexler, Thermodynamic model of the system $H^+ - NH_4^+ - SO_4^{2-} - NO_3^- - H_2O$ at tropospheric temperatures, *J. Phys. Chem. A*, 1998, **102**, 2137–2154.

61 M. Shiraiwa, C. Pfrang and U. Pöschl, Kinetic multi-layer model of aerosol surface and bulk chemistry (KM-SUB): the influence of interfacial transport and bulk diffusion on the oxidation of oleic acid by ozone, *Atmos. Chem. Phys.*, 2010, **10**, 3673–3691.

62 U. Pöschl, Y. Rudich and M. Ammann, Kinetic model framework for aerosol and cloud surface chemistry and gas-particle interactions - Part 1: General equations, parameters, and terminology, *Atmos. Chem. Phys.*, 2007, **7**, 5989–6023.

63 J. Mao, S. Fan, D. J. Jacob and K. R. Travis, Radical loss in the atmosphere from Cu-Fe redox coupling in aerosols, *Atmos. Chem. Phys.*, 2013, **13**, 509–519.

64 L. Deguillaume, M. Leriche, K. Desboeufs, G. Mailhot, C. George and N. Chaumerliac, Transition metals in atmospheric liquid phases: Sources, reactivity, and sensitive parameters, *Chem. Rev.*, 2005, **105**, 3388–3431.

65 A. N. Pham, G. Xing, C. J. Miller and T. D. Waite, Fenton-like copper redox chemistry revisited: Hydrogen peroxide and superoxide mediation of copper-catalyzed oxidant production, *J. Catal.*, 2013, **301**, 54–64.

66 J. D. Rush and B. H. Bielski, Pulse radiolytic studies of the reaction of perhydroxyl/superoxide O2-with iron (II)/iron (III) ions. The reactivity of HO2/O2-with ferric ions and its implication on the occurrence of the Haber-Weiss reaction, *J. Phys. Chem.*, 1985, **89**, 5062–5066.

67 S. P. Sander, R. R. Friedl, D. M. Golden, M. J. Kurylo, R. E. Huie, V. L. Orkin, G. K. Moortgat, A. R. Ravishankara, C. E. Kolb, M. J. Molina and B. J. Finlayson-Pitts, *Chemical Kinetics and Photochemical Data for Use in Atmospheric Studies*, JPL Publication, 2003, vol. 14.

68 T. A. Staffelbach and G. L. Kok, Henry law constants for aqueous solutions of hydrogen peroxide and hydroxymethyl hydroperoxide, *J. Geophys. Res.: Atmos.*, 1993, **98**, 12713–12717.

69 J. Casas, F. Alvarez and L. Cifuentes, Aqueous speciation of sulfuric acid–cupric sulfate solutions, *Chem. Eng. Sci.*, 2000, **55**, 6223–6234.

70 P. T. Griffiths and R. A. Cox, Temperature dependence of heterogeneous uptake of N_2O_5 by ammonium sulfate aerosol, *Atmos. Sci. Lett.*, 2009, **10**, 159–163.

71 R. G. Remorov, Y. M. Gershenzon, L. T. Molina and M. J. Molina, Kinetics and mechanism of HO_2 uptake on solid NaCl, *J. Phys. Chem. A*, 2002, **106**, 4558–4565.

72 E. Loukhovitskaya, Y. Bedjanian, I. Morozov and G. Le Bras, Laboratory study of the interaction of HO_2 radicals with the NaCl, NaBr, $MgCl_2 \cdot 6H_2O$ and sea salt surfaces, *Phys. Chem. Chem. Phys.*, 2009, **11**, 7896–7905.

73 G. M. Nathanson, P. Davidovits, D. R. Worsnop and C. E. Kolb, Dynamics and kinetics at the gas-liquid interface, *J. Phys. Chem.*, 1996, **100**, 13007–13020.

74 D. A. Knopf, M. Ammann, T. Berkemeier, U. Pöschl and M. Shiraiwa, *Desorption Lifetimes and Activation Energies*

Influencing Gas-Surface Interactions and Multiphase Chemical Kinetics, EGUsphere, 2023, vol. 2023, pp. 1–140.

75 P. S. J. Lakey, T. Berkemeier, H. Tong, A. M. Arangio, K. Lucas, U. Pöschl and M. Shiraiwa, Chemical exposure-response relationship between air pollutants and reactive oxygen species in the human respiratory tract, *Sci. Rep.*, 2016, **6**, 32916.

76 Y. Gao, S. Yu, R. M. Sherrell, S. Fan, K. Bu and J. R. Anderson, Particle-size distributions and solubility of aerosol iron over the Antarctic peninsula during austral summer, *J. Geophys. Res.: Atmos.*, 2020, **125**, e2019JD032082.

77 M. R. Goforth and C. S. Christoforou, Particle size distribution and atmospheric metals measurements in a rural area in the South Eastern USA, *Sci. Total Environ.*, 2006, **356**, 217–227.

78 L. Liu, W. Li, Q. Lin, Y. Wang, J. Zhang, Y. Zhu, Q. Yuan, S. Zhou, D. Zhang and C. Baldo, Size-dependent aerosol iron solubility in an urban atmosphere, *npj Clim. Atmos. Sci.*, 2022, **5**, 53.

79 E. Bjergbakke, K. Sehested and O. L. Rasmussen, The reaction mechanism and rate constants in the radiolysis of solutions, *Radiat. Res.*, 1976, **66**, 433–442.

80 D. Stone and D. M. Rowley, Kinetics of the gas phase HO_2 self-reaction: Effects of temperature, pressure, water and methanol vapours, *Phys. Chem. Chem. Phys.*, 2005, **7**, 2156–2163.

81 X. Xu and W. A. Goddard, Peroxone chemistry: formation of H_2O_3 and ring-$(HO_2)(HO_3)$ from O_3/H_2O_2, *Proc. Natl. Acad. Sci. U. S. A.*, 2002, **99**, 15308–15312.

82 H. Song, K. Lu, H. Dong, Z. Tan, S. Chen, L. Zeng and Y. Zhang, Reduced aerosol uptake of hydroperoxyl radical may increase the sensitivity of ozone production to volatile organic compounds, *Environ. Sci. Technol. Lett.*, 2021, **9**, 22–29.

83 M. Jingqiu and F. Songmiao, *Soluble Fe in Aerosols Sustained by Gaseous HO2 Uptake*, 2017.

84 A. Khaled, M. Zhang and B. Ervens, The number fraction of iron-containing particles affects OH, HO2 and H2O2 budgets in the atmospheric aqueous phase, *Atmos. Chem. Phys.*, 2022, **22**, 1989–2009.